Published in: Advanced Electronic Materials, Vol. 4, No. 6, 1700562, DOI: 10.1002/aelm.201700562, Jun 2018

Full Paper

Mechanisms for Enhancing Polarization Orientation and Piezoelectric Parameters of PVDF Nanofibers

Yasmin Mohamed Yousry[1,2], Kui Yao[1], Shuting Chen[1], Weng Heng Liew[1,2], and Seeram Ramakrishna[2]*

Y. M. Yousry, Dr. K. Yao, Dr. S. Chen, W. H. Liew,
Institute of Materials Research and Engineering, A*STAR (Agency for Science, Technology and Research), 2 Fusionopolis Way, Innovis, 138634, Singapore
E-mail: k-yao@imre.a-star.edu.sg
Y. M. Yousry, Prof. S. Ramakrishna
Department of Mechanical Engineering, National University of Singapore, 9 Engineering Drive 1, 117575, Singapore

Keywords: piezoelectric, polarization, electromechanical, PVDF, nanofibers

Many emerging applications strongly demand flexible and efficient electromechanical conversion materials. Polymeric piezoelectric materials, with ability of large area and low temperature processing are attractive to obtain wide applications for electromechanical sensors, transducers and mechanical energy harvesters. A major drawback of the polymeric piezoelectric materials is their much lower piezoelectric performance property, such as piezoelectric strain coefficient, than their ceramic counterparts. Here outstanding piezoelectric performance properties with giant effective strain and voltage coefficients of −116 pm V^{-1} and −1180 V mm N^{-1} have been achieved in electrospun polyvinylidene fluoride (PVDF) nanofiber films from the precursor solution modified with hydrated salt. Our experimental results and theoretical analysis clarify a synergistic interactive role from the hydrated salt and the electric field during electrospinning effectively leading to polarization enhancement and alignment, and hence the giant macroscopic piezoelectric coefficients in the obtained electrospun fiber films. The demonstrated results and the understanding on the underlying mechanism exhibit the potential and strategy in achieving high performance functional materials through dedicated control on their nanostructures and polarizations.

Published in: Advanced Electronic Materials, Vol. 4, No. 6, 1700562, DOI: 10.1002/aelm.201700562, Jun 2018

1. Introduction

Emerging applications in the fields of tactile, wearable devices, and implanted medical electronics strongly demand flexible and high performance piezoelectric materials that provide inherent and efficient electromechanical coupling. [1-3] Polymeric piezoelectric materials have several advantages over ceramic. They are flexible, can be deposited in large area by scalable and low-cost manufacturing process at much lower processing temperature, and can be formed easily into desired shapes. [4] Piezoelectric polymers were earliest reported in 1924 by Brain who found piezoelectricity in glass, ebonite, sealing wax, celluloid, rubber, and hard paraffin. [5] In 1941, Martin presented piezoelectricity in aligned human hair. [5] In 1950, quantitative studies on the piezoelectricity of wood were originated by Bazhenov and Konstantinova. [4] In 1957, Fukada and Yasuda found shear piezoelectricity in bone. [5] Fukada extended the research on shear piezoelectricity to many kinds of polymers such as polysaccharide, proteins and synthetic polymers. [6] Strong piezoelectric effect in polar polymers was first revealed by Kawai in 1969 by drawing and poling a polyvinylidene fluoride (PVDF) film, [7] followed by reports of piezoelectric effect in polyvinylchloride, polycarbonate, and nylon 11. [8] Currently, PVDF and its copolymers are the most technically important piezoelectric polymers. [2]

PVDF is a semi-crystalline polymer consists of a repeated monomer unit of -CH_2-CF_2- which is characteristically polar because of the electropositive hydrogen atoms and the electronegative fluorine atoms in contrast to the carbon chain. [7] PVDF exhibits four crystalline phases, designated as α, β, γ and δ. [8] Among those phases, β phase has the largest spontaneous polarization, exhibiting the most significant ferroelectric and piezoelectric effects. [9] The piezoelectric strain and voltage coefficients (such as d_{33} and g_{33}) are often used as the metrics for evaluating piezoelectric property. Typically, β-phase PVDF polymers exhibit a d_{33} value of about −25 to −35 pm V^{-1}. Theoretical study on PVDF has suggested that

Published in: Advanced Electronic Materials, Vol. 4, No. 6, 1700562, DOI: 10.1002/aelm.201700562, Jun 2018

equivalent macroscopic piezoelectric d_{33} value could possibly reach −186 pm V^{-1}, but this has not been achieved experimentally. [10]

As α phase is the thermodynamic stable crystalline phase, to improve piezoelectric performance of PVDF, many studies focus on enhancing the polar phase formation through various techniques, such as mechanical stretching, [7] high electrical field poling, [11] melting and crystallization under high pressure, [12] electrospinning, [3] and use of additives including hydrated salts, [13] clay, [14] ferrite nanoparticles and carbon nanotubes (CNTs). [15] Among them, introducing hydrated salts in PVDF precursor solution proves very effective in improving the content of polar β phase, promoted by hydrogen bonds formation between fluorine and hydroxyl group in the hydrated salts. [13,16,17] On the other hand, it is noted that the structure and piezoelectric properties of PVDF can be manipulated through nanoscale fabrication, [18,19] among which electrospinning process stands out as a simple, versatile, and scalable process. [20, 21] Electrospinning system consists of three major components: a high voltage power supply, a syringe pump, and a collector. [22] The electrospinning process for fabricating PVDF involves drawing a viscous PVDF solution under a strong electric field to form piezoelectric nanofibers with polar phase transformation. [23] The previous studies have also shown that the piezoelectric sensors made of PVDF electrospun fibers from a solution with polar additives including hydrated salts possess enhanced electrical output, [20-21] but the underlying material mechanism is unclear and how large of the piezoelectric parameters of the electrospun PVDF materials are not determined.

Here, PVDF nanofibers are fabricated with our dedicatedly designed method by electrospinning our previously optimized solutions with aluminium nitrate nonahydrate salt ($Al(NO_3)_3.9H_2O$). [17] Unprecedentedly large effective piezoelectric strain and voltage coefficients ($d_{33\,(eff)}$ = −116 pm V^{-1} and $g_{33\,(eff)}$ = −1180 V mm N^{-1}) are achieved. Our theoretical analysis and experimental results show an interesting synergistic effect between the electrospinning process and the hydrated salt, which not only greatly promotes β-phase

Published in: Advanced Electronic Materials, Vol. 4, No. 6, 1700562, DOI: 10.1002/aelm.201700562, Jun 2018

formation but also enhances the polarization alignment in the resulting PVDF nanofibers. The achieved outstanding piezoelectric parameters and understanding on the mechanism will inspire applications of electrospun PVDF polymer nanofiber material for various electromechanical sensors and transducers applications.

2. Results and discussion

2.1. Surface morphology

Figure 1(a), (b) and **(c)** show the surface morphology of the obtained fibers from the PVDF homopolymer solutions with 0 wt%, 8 wt% and 16 wt% (Al $(NO_3)_2 \cdot 9H_2O$) salt, respectively. Introducing the hydrated salt (8 wt%) to the PVDF solution reduced fibers diameter and eliminated beads formation, which is attributed to the higher charge density in the electrified jet of the polymer solution containing the salt resulting in a larger elongation. The volume content of the pores is 44 % calculated from the volume of the film and the density of the fiber with 8 wt% salt added to the precursor solution, and the average pore size is around 1 μm as measured by DiameterJ software. With the excessive addition of salt (16 wt%), aggregation of the fibers was observed, as shown in Figure 1(c). Such aggregation is reported, according to a study with lithium perchlorate as a salt additive, as a result of accelerated gelation behaviour of PVDF in water / DMF solutions. [24] The too high charge density due to the over high concentration of salt increases the attraction of the electrospinning jet towards the grounded collector, which may lead to shorter flight duration and less stretched fibers with larger diameter.

2.2. Crystalline structure

The effect of the electrospinning process and the addition of Al $(NO_3)_3 \cdot 9H_2O$ salt on the crystalline phases of the PVDF polymer was investigated using both X-ray diffraction (XRD)

Published in: Advanced Electronic Materials, Vol. 4, No. 6, 1700562, DOI: 10.1002/aelm.201700562, Jun 2018

and Fourier transform infrared (FTIR) spectroscopy. **Figure 2(a)** shows the attenuated total reflection (ATR) FTIR spectra of PVDF films deposited by electrospinning and spin-coating process with and without the addition of salt. The distinctive absorption bands of the non-polar α phase are located at 764 and 975 cm^{-1}, [25] while the distinctive absorption bands of the polar β phase located at 840, and 1276 cm^{-1}. [26] The FTIR spectra of the electrospun fibers show increase in the intensity of the absorption bands of both α and β phases compared to spin-coated films from the same solution (PVDF without and with 8 wt% (Al $(NO_3)_3 \cdot 9H_2O$)). As suggested by previous study, the higher crystallinity in electrospun PVDF fibers arises from the favoured orientation of the polymer chains along the nanofibers direction caused by the stretching electrospun jet under high electrical field simultaneously. [14] It is also observed that the intensity of α-phase peaks is suppressed while that for β-phase peaks is enhanced with the salt added for both electrospinning and spin-coating process, which is due to the hydrogen bond between the water of crystallization and fluorine. [13,16] Figure 2(b) compares the XRD spectra of PVDF films deposited by spin-coating and electrospinning process from the same polymer solutions with and without the addition of 8 wt% salt. PVDF has characteristic XRD peaks at $2\theta = 17.66°$ and 20.1° corresponding to (100) and (110) crystal planes of α phase, and at $2\theta = 20.8°$ corresponding to the sum of (110) and (200) plane reflections of β phase. [27] For using the solution without the addition of the salt, the XRD patterns as presented reveal the coexistence of α and β phases in both spin-coated and electrospun samples, but the intensity of β phase is higher while α phase is lower in the electrospun sample compared to the spin-coated samples. With the addition of the salt in the solution (8 wt% Al $(NO_3)_3 \cdot 9H_2O$), the electrospun PVDF fibers only show sharp β-phase reflections without substantial α phase. All these results and analyses show that both electrospinning process and the addition of $Al(NO_3)_3 \cdot 9H_2O$ salt to PVDF solutions promote β phase while suppress α phase, and electrospinning of PVDF solution with the addition of $Al(NO_3)_3 \cdot 9H_2O$ will lead to β-phase nanofibers with enhanced crystallinity.

Published in: Advanced Electronic Materials, Vol. 4, No. 6, 1700562, DOI: 10.1002/aelm.201700562, Jun 2018

The molecular orientation in the electrospun PVDF fibers in comparison with spin-coated PVDF film was examined by polarized FTIR spectra. **Figure 3(a)** shows the polarized FTIR spectra in which an enhanced absorption peak appears when the molecular vibration and the electric field component of the incident IR are parallel to each other. The absorption bands at 1288 cm^{-1} (ν_s *(*CF_2*)*, symmetric stretching vibration of CF_2 groups with dipole transition moment parallel to the polar *b* axis) is much weaker in the spectrum of the electrospun fibers than that for the spin-coated film. This indicates that the polar *b* axis of the electrospun PVDF fibers is largely perpendicular to the substrate, which is reoriented under the electrospinning field pointing to the substrate during fiber deposition. [3,26] Additionally, the most intense bands in the electrospun fibers appear at 1400 cm^{-1} (*w (*CH_2*),* wagging vibration of CH_2 groups with dipole transition moment parallel to the *c* axis along the polymer chain) and at 1187 cm^{-1} (ν_a *(*CF_2*),* antisymmetric stretching vibration of CF_2 groups and *r (*CF_2*),* rocking vibration of CF_2 groups with dipole transition moments parallel to the *a* axis), which indicate that the polymer chains were oriented parallel to the substrate. [18]

To further verify this result, the ψ dependence of the XRD peak intensity was investigated for the electrospun fibers in comparison with the spin-coated film, in which ψ is the incline angle between the sample surface and the normal of the crystal planes. As shown in Figure 3(b), the diffraction peak intensity of the electrospun PVDF fibers strongly relies on ψ, showing the maximum at ψ = -90 for β-phase reflections (200)/(110), while the peak intensity does not vary substantially with ψ for the spin-coated PVDF film. Since the crystal planes of β phase (200)/(110) are parallel to the molecular chains, the result indicates that the molecular chains were oriented in parallel with the substrate . This result verifies the effect of the electrospinning process in aligning the dipoles of β-phase crystallites perpendicular to substrate and the fiber axis.

Figure S1 (Supporting Information) present the FTIR spectra of electrospun PVDF fibers, derived from the solutions with 0, 8, 10, 12, 14, and 16 wt% $Al(NO_3)_3 \cdot 9H_2O$, showing

Published in: Advanced Electronic Materials, Vol. 4, No. 6, 1700562, DOI: 10.1002/aelm.201700562, Jun 2018

that electrospun PVDF fibers have single crystalline polar β phase with the addition of salt with different concentrations. However, with very high amount of salt such as 16 wt%, the β phases decreased due to the aggregation of the fibers, as observed with FESEM (Figure 1(c)).

2.3. Dielectric Properties

Figure 4 shows the dielectric constant and dielectric loss of the electrospun PVDF fibers as a function of Al $(NO_3)_3 \cdot 9H_2O$ concentration. The obtained data points were connected with modified Bezier fitting curves, which give smooth polygon shape-preserving connections. The dielectric constant increases with the increase in salt concentration and reaches the highest value of 11.1 at 10 wt% salt. The variation trend in dielectric loss with salt concentration is inverse to that of the dielectric constant, with the minimum value of dielectric loss of 0.0023 obtained at 10 wt% salt in contrast to the significantly larger loss in the samples without and with over amount of hydrated salt. The increase in dielectric loss with higher salt concentration such as 14 and 16 wt% is believed due to the residual of the excessive hydrated salt and the degraded morphology as described above.

Figure S2 (Supporting Information) presents the details about the dependence of the dielectric constant and loss of the electrospun PVDF fibers on the salt concentration measured at room temperature over frequency range of 1 kHz to 1 MHz. It is observed that the dielectric constant of all the samples decreases with increasing frequency, which is due to dielectric relaxation. [28] It is noted that the optimized electrospun PVDF fibers, with 10 wt% Al $(NO_3)_3 \cdot 9H_2O$ possess stable dielectric constant and maintain low dielectric loss over a broad frequency range up to MHz. The dielectric breakdown field for the fiber films was observed in the range from 430 to 450 MV/m.

2.4. Piezoelectric properties

Published in: Advanced Electronic Materials, Vol. 4, No. 6, 1700562, DOI: 10.1002/aelm.201700562, Jun 2018

The laser scanning vibrometer (LSV) technique was used to detect the displacement of both the electrically excited area (under the top electrode with 1 mm diameter) and the substrate concurrently to determine the dilatation in thickness direction of the PVDF fiber films due to piezoelectric response. The LSV testing was conducted with a unipolar sine wave voltage of 30 V in amplitude at 10 kHz applied to the samples. **Figure 5(a)** presents a three-dimensional graph of the instantaneous vibration data when the displacement magnitude of a PVDF fiber film reaches the maximum with the electric sine wave driving. The tested PVDF electrospun fiber sample was prepared from solution with 10 wt% $Al(NO_3)_3 \cdot 9H_2O$ salt without post-poling step. The central protruding area is the electrically excited Al top electrode covering the fibers, whereas the flat adjacent area is the PVDF fibers without the top electrode. The average value over the top area rather than the highest point is used for calculating the effective piezoelectric strain coefficient $d_{33\,(eff),}$ which is −116 pm V^{-1} under the substrate clamping condition. The corresponding effective piezoelectric voltage coefficient $g_{33\,(eff)}$ reaches −1180 V mm N^{-1}. The effective $d_{33\,(eff)}$ values of electrospun PVDF fibers derived from solutions with different salt concentrations are provided in Figure 5(b), with the data points connected with modified Bezier fitting curve. The trend shows the increase in $d_{33\,(eff)}$ with the addition of salt till the maximum value of −116 pm V^{-1} obtained in the sample prepared with the addition of 10 wt% salt. With further increase in the salt concentration above 10 wt% the effective piezoelectric coefficient degrades again, which is consistent with the results of the degraded crystalline structure and dielectric properties with excessive hydrated salt.

In order to confirm the obtained spectacular effective piezoelectric performance through the converse piezoelectric effect, a direct piezoelectric effect measurement approach using a vibrational shaker testing apparatus was adopted to evaluate piezoelectric coefficient d_{33} by converting mechanical energy to electrical energy, as shown in **Figure S3 (Supporting Information)**. The piezoelectric electrospun PVDF fiber film (from 10 wt% salt) was

Published in: Advanced Electronic Materials, Vol. 4, No. 6, 1700562, DOI: 10.1002/aelm.201700562, Jun 2018

sandwiched between top Al electrode with a mass load (weight of 0.012 Kg) and bottom electrode to generate electrical output in response to mechanical vibration from the shaker driven by a power amplifier and function generator. The acceleration was measured with an accelerator and confirmed by LSV measurement. The piezoelectric output under mechanical vibration at 100 Hz is shown in Figure 5(c). With an acceleration magnitude of 0.015 m s^{-2}, the average output voltage was ~100 mV. The piezoelectric voltage output can be expressed as: [29]

$$V = -\frac{d_{33} Mah}{\varepsilon_{33} A} \quad (1)$$

where V is the output voltage (100 mV), M is the mass load (0.012 Kg), a is the acceleration (0.015 m s^{-2}), h is the film thickness (20 μm), ε_{33} is the dielectric permittivity (11.1 x 8.85 x 10^{-12} C^2 N^{-1} m^{-2}), and A is the cross-sectional area (0.5 cm^{-2}). The outstandingly large $d_{33\,(eff)}$ value calculated from direct piezoelectric effect with **Equation (1)** is −123 pm V^{-1} under the substrate clamping effect, which is consistent with the value measured from the converse piezoelectric effect by LSV.

Figure 5(d) provides d_{33} values reported for various PVDF films prepared with different methods and characterized by three techniques. d_{33} meter or "Berlincourt piezometer" is used as one measurement method in which the sample is clamped and dynamically loaded by the upper-force head of the piezometer to generate a voltage pulse for the measurement. [29] As shown in Figure 5(d), the maximum value of d_{33} was ~26 pm V^{-1} in a PVDF thick film under substrate clamping. [30] The drawback of measuring d_{33} for the soft polymer films by this method is the difficulty to produce a homogeneous uniaxial stress on the film without creating a bending effect. Piezoresponse force microscopy (PFM) is used for measuring d_{33} at nanoscales, [33] in which the local displacement is induced and detected by a PFM probe. [34] By PFM measurements, electrospun PVDF fibers have been reported with different d_{33} values. As shown in Figure 5(d), the maximum reported d_{33} value was ~63 pm V^{-}

Published in: Advanced Electronic Materials, Vol. 4, No. 6, 1700562, DOI: 10.1002/aelm.201700562, Jun 2018

[1] for electrospun PVDF fibers processed by near-field electrospinning (NFES). [35] Quantitative determination of d_{33} value by PFM is difficult due to the unknown substrate bending effect and non-uniform local electric field. A reliable and efficient measuring method is using LSV technique for determining the piezoelectric dilatation of the film by monitoring and separating bending of the substrate over a large area. [40] Measured by LSV method, the highest d_{33} value was −19.2 pm V^{-1} for PVDF homopolymer.[41] Here, we obtain the outstandingly large $d_{33\,(eff)}$ value of −116 pm V^{-1} in electrospun PVDF fiber film as measured by LSV and further verified by direct piezoelectric voltage output measurement, which is significantly higher than various PVDF homopolymer materials as reported in the literature. Furthermore, nanoindentation test was performed to measure the elastic modulus of the fiber films, with the test repeated at ten different locations in the films. The median value of the elastic modulus was estimated as 230 MPa with a standard deviation of 73 MPa for the fiber film with 10 wt. % salt added in the precursor solution, while 500 MPa with a standard deviation of 123 MPa for the fiber film without salt. The experimental data revealed that the addition of salt decreases the elastic modulus due to the enhancement of the crystalline phase and the reduction of the denser amorphous phase, as revealed by the XRD and FTIR results in Figure 2 (a) and (b).

To further validate the obtained outstanding $d_{33\,(eff)}$ values, efforts were made to exclude the possible effects of large samples defects like delamination on the displacement measurements. Ultrasonic scanning microscopy using a 100 MHz piezoelectric transducer was conducted to examine the adhesion of the electrospun PVDF fibers on the substrate. The experimental set-up with the sample immersed in a water tank for the ultrasonic scan and the obtained ultrasonic images are presented in **Figure S4 (Supporting Information)**, showing homogeneous adhesion between the film and the substrate. Cross-sectional FESEM examination does not reveal obvious delamination, as shown in **Figure S5 (Supporting Information)**.

Published in: Advanced Electronic Materials, Vol. 4, No. 6, 1700562, DOI: 10.1002/aelm.201700562, Jun 2018

3. Theortical Analysis

Since the discovery of piezoelectric effect in PVDF, the origin of piezoelectricity and theoretical limit of piezoelectric properties have been controversial for a long time. According to the theoretical analysis carried out by K. Tashiro, et.al. in 1980, by considering each atom as an effective point charge and neglecting the electrostatic long-range interactions in the PVDF β-phase crystal, the estimated d_{33} coefficient was −25 pm V^{-1}. [42] In 1982, the same group modified their model to investigate the macroscopic piezoelectric constants by taking into account other factors such as the content of polar phase, the degree of dipole orientation along the electric field, the electrostriction constant and the coupling effect of the amorphous and crystalline phases. [10] The estimated theoretical limit of the macroscopic piezoelectric constant d_{33} was −186 pm V^{-1} , the contribution of the intrinsic piezoelectric effect of the crystal is - 31.5 pm V^{-1}. In 1998, W. Eisenmenger et.al studied experimentally the role and the interaction of space charges and dipoles in electret PVDF, and they concluded that the injection of ionic space charge during the poling process plays the dominant role for PVDF polarization enhancement. [43] Under high electric field strength of the poling process, electrons (or holes) are injected by tunnelling from metal electrodes to the PVDF film creating charged localized states which cause splitting off ions in the polymer chains. [44,45] This indicates that not only dipoles in the crystals, but also the injected charges in PVDF make significant contributions to its piezoelectric property. However, as shown in Figure 5(d), d_{33} value as obtained in experiment is always far below the theoretically predicted limit.

In this work, the effective piezoelectric coefficient $d_{33(eff)}$ of the fiber film with the hydrated salt is -116 pm V^{-1}, while for the spin coated film it is -14.5 pm V^{-1}. [2] While the improved polar phase crystallinity does increase the intrinsic part of $d_{33(eff)}$, the huge enhancement by ~800 % may largely be attributed to extrinsic effect. Here the extrinsic

Published in: Advanced Electronic Materials, Vol. 4, No. 6, 1700562, DOI: 10.1002/aelm.201700562, Jun 2018

effects may be related to the changes in the dielectric and mechanical properties between a solid film and a porous nanofiber film. For example, the $d_{33(eff)}$ of the fiber films with 10 wt. % and 16 wt.% salt are -116 pm/V and -78 pm/V, respectively, without much difference in their crystallinity. The large difference between these two samples can only be attributed to the decreased void formation of the sample with 16 wt. % salt. This means that at least 30 % of $d_{33(eff)}$ enhancement is just due to the variation in the charged voids. While we understand improving the crystallinity of polar phase is important to enhance the formation of charged pores with space charge dipoles, there is a big room to play to further improve the $d_{33(eff)}$ value by controlling the porous structure of the nanofiber films.

It has been understood that the addition of $Al(NO_3)_3 \cdot 9H_2O$ salt in PVDF solution enhances the polar β-phase content due to the formation of hydrogen bonds (dipole-dipole interactions) between the water molecules of the hydrated salts and the $–CF_2$ dipoles of the PVDF chains, [16] besides ion-dipole interactions between the metal ions in the salt and the polymer dipoles, as schematically illustrated in **Figure 6(a)**. Thus, the highly polar PVDF can be much more effectively reoriented under the high electric field applied during the electrospinning process. Such a synergistic interaction from the hydrated salt induced polar configuration and electric field induced orientation of the polar structure results in the electrospun fiber films with the polar *b* axis perpendicular to the substrate, as proved by the ψ dependence of the XRD peak and the polarized FTIR (Figure 3(a) and (b)). The aligned dipoles in the nanofibers can generate boundaries with the polarity charges at the fiber surfaces, where a large amount of space charges are bonded to form charged voids and electret dipoles between these polarized fibers, as illustrated in Figure 6(b) and (c). The piezoelectric response can be enhanced by the contribution from the space charge dipoles in addition to the pre-existing β-phase dipoles. The effective piezoelectric response of charged pores known as piezo-electrets exists in many cellular piezoelectric polymers. [46] In this study, the electret dipoles in the charged voids of the electrospun fibers can be well aligned

Published in: Advanced Electronic Materials, Vol. 4, No. 6, 1700562, DOI: 10.1002/aelm.201700562, Jun 2018

perpendicular to the film without any poling treatment, same as the aligned β-phase dipoles, under the synergistic interaction from the hydrated salt and the electric field during the electrospinning process. All the highly oriented polar structures contribute to the significantly enhanced macroscopic piezoelectric performance properties as observed in the electrospun nanofiber films.

4. Conclusion

Outstanding piezoelectric performance properties with giant effective strain and voltage coefficients, $d_{33\,(eff)}$ of −116 pm V^{-1} and $g_{33\,(eff)}$ of −1180 V mm N^{-1}, were achieved in electrospun PVDF homopolymer nanofiber films from the precursor solution with $Al(NO_3)_3 \cdot 9H_2O$. The piezoelectric material parameters were obtained over a macroscale using both laser scanning vibrometer through the converse piezoelectric effect and mechanical shaker through the direct piezoelectric effect. Our theoretical analysis showed a synergistic interactive mechanism, wherein the hydrated salt added in the solution induces polar configuration and the electric field during electrospinning induces orientation of the polar structure, leads to the electrospun fiber films with the polar axis perpendicular to the substrate, as evidenced with experimental results. Electret dipoles in the charged voids of the electrospun fibers can be aligned perpendicular to the film as well without any poling treatment, as the polar phase dipoles aligned under the cooperative interaction from the hydrated salt and the electric field during the electrospinning process. All the highly oriented polar structures contribute to the significantly enhanced macroscopic piezoelectric performance properties in the electrospun nanofiber films. With the large effective piezoelectric strain coefficient even comparable with ceramic, and advantages of flexible, eco-friendly, low cost, and easy to be processed over large area at low temperature, the electrospun PVDF nanofibers are promising for many electromechanical system applications,

Published in: Advanced Electronic Materials, Vol. 4, No. 6, 1700562, DOI: 10.1002/aelm.201700562, Jun 2018

including sensors, transducers, and mechanical energy harvesters. The synergistic interactive mechanism involving inducing polar configuration followed by polarization orientation shows an effective strategy in achieving superior performance in polarization-critical functional materials.

5. Experimental Section

Materials: Different concentrations of PVDF precursor solutions were prepared by dissolving PVDF (540,000 MW, Sigma-Aldrich) in a solvent composed of 80 wt% dimethylformamide (DMF, TEDIA) and 20 wt% acetone (J. T. Baker). For smooth electrospinning process, it was found that the appropriate PVDF concentration was 15 wt% while lower and higher PVDF concentrations do not show suitable viscosity. Aluminium nitrate nonahydrate salt ($Al(NO_3)_2 \cdot 9H_2O$, Sigma-Aldrich) was added to the PVDF solution with different concentrations (8, 10, 12, 14, and 16 wt%) in percentage weight of the PVDF polymer. The solutions were heated at 55 °C in silicone oil bath for 2 hours to completely dissolve the polymer until get a clear transparent solution.

Electrospinning deposition: The PVDF solution was loaded in a 3-mL plastic syringe capped with a 21-gauge stainless steel needle (inner diameter = 0.82 mm). A high voltage of 15 kV was applied to the needle through a DC power supply (Gamma High Voltage, AU-30P1-L220V, Japan). The solution was injected from the needle at a constant rate of 0.5 mL/h with a syringe pump (SP100IZ Syringe Pump, 789100W, U.S.A). A static collector made of a metallic plate covered with an Al foil was grounded and used as the fiber collector substrate. The process was carried out at room temperature and 45% RH to prevent solution gelation at the needle tip.

The wet films were dried on a hotplate at 100 °C for 10 minutes then annealed at 135 °C for 12 hours in an oven. The thickness of the films was fixed at 20 μm by controlling the deposition parameters of the electrospinning process. Patterns of top electrodes (150 nm thick

Published in: Advanced Electronic Materials, Vol. 4, No. 6, 1700562, DOI: 10.1002/aelm.201700562, Jun 2018

aluminium) were deposited on the films by e-beam evaporator to serve for the electrical measurements.

Characterizations: The surface morphology was examined using a field emission scanning electron microscopy (FESEM, JSM-6700F, JEOL). The crystalline structure analysis was performed at room temperature using an x-ray diffraction (XRD system D8-ADVANCE, Bruker AXS GmbH, Karlsruhe, Germany) and Fourier transform infrared (FTIR spectroscopy Spectrum 2000, Perkin Elmer). Nanoindentation test was performed with Aglient G200 system with an indentation depth of 2 μm to determine the elastic modulus. The frequency dependent dielectric properties of the films were analysed by an impedance analyser (Agilent 4294A). The piezoelectric property was measured by a laser scanning vibrometer (OFV-3001-SF6, PolyTech GmbH, Germany) and verified by vibrational shaker (TIRA TV 51110 from TIRA GmbH) testing in which a power amplifier (TIRA BAA 120) was used to excite the shaker and an accelerator (4525B-51049 from Brüel and Kjær) was used to measure the acceleration..

Supporting Information
Supporting Information is available from the Wiley Online Library or from the author.

Acknowledgements
The authors acknowledge the research grant support in part by the Singapore Maritime Institute under the Asset Integrity & Risk Management (AIM) R&D Programme, Project ID: SMI-2015-OF-01, and IMRE/15-9P1115.

The work was designed by K. Yao, Y. M. Yousry and S. Ramakrishna. Preparing materials and carrying out experiments were done by Y. M. Yousry. W. H. Liew assisted in the electrical characterization and the ultrasonic imaging. K. Yao, Y. M. Yousry and S. Chen did the analysis and discussion of the results. All the authors contribute in writing and revising the manuscript.

Received:
Revised:
Published online:

Published in: Advanced Electronic Materials, Vol. 4, No. 6, 1700562, DOI: 10.1002/aelm.201700562, Jun 2018

References

[1] K. Uchino, *Advanced Piezoelectric Materials: Science and Technology*, Duxford, United Kingdom, Woodhead **2017**.

[2] H. Wu, Y. A. Huang, F. Xu, Y. Duan, Z. Yin, *Adv. Mater.* **2016**, *28*, 9881.

[3] P. Luana, D. Canan, S. Yewang, D. Pisignano, Y. Huang, A. J. Rogers, *Nat. Commun.* **2013**, *4*, 1633.

[4] Y. Bar-Cohen, Q. Zhang, *MRS Bull.* **2008**, *33*, 173.

[5] E. Fukada, *IEEE Trans. Dielectr. Electr. Insul.* **2006**, *13*, 110.

[6] A. J. Lovinger, *Science* **1983**, *220*, 1115.

[7] H. Kawai, *Jpn. J. Appl. Phys.* **1969**, *8*, 975.

[8] H. Nalwa, *Ferroelectric Polymers*, New York: Marcel Dekker, Inc. **1995**.

[9] L. Mengyuan, J. W. Harry, S. Mark-Jan, A. Kamal, K. Ilias, W. M. B. Paul, M. D. L. Dago, *Nat. Mater.* **2013**, *12*, 433.

[10] K. Tashiro, H. Tadokoro, *Macromolecules* **1983**, *16*, 961.

[11] A. Kumart, M. M. Perlman, *J. Phys. D: Appl. Phys*. **1993**, *28*, 469.

[12] H. Ohigashi, T. Hattori, *Jpn. J. Appl. Phys*. **1989**, *28*, L1612.

[13] X. He, K. Yao, *Appl. Phys. Lett*. **2006**, *89*, 1.

[14] Y. L. Liu, Y. Li, J. T. Xu, Z. Q. Fan, *ACS Appl. Mater. Interfaces* **2010**, *2*, 1759.

[15] W. A. Yee, J. Kong, C. Zhang, T. Liu, M. Kotaki, X. Lu, *Polymer* **2012**, *53*, 5097.

[16] S. Chen, K. Yao, F. E. H. Tay, C. L. Liow, *J. Appl. Phys.* **2007**, *102*, 104.

[17] X. Li, S. Chen, K. Yao, F. E. H. Tay, *J. Polym. Sci. B Polym. Phys.* **2009**, *47*, 2410.

[18] W. H. Liew, M. S. Mirshekarloo, S. Chen, K. Yao, F. E. H. Tay, *Sci. Rep*. **2015**, *5*, 1.

[19] K. Mehmet, A. Ozan, S. S. Huseyin, D. Engin, *ACS Nano* **2014**, *8*, 9311.

[20] D. Dipti, B. Vivek, O. Satishchandra, J. Jyoti, *Nanoscale* **2012**, *4*, 752.

[21] Y. Bin, M. Mengye, Y. Hao, H. Tao, Z. Weiwei, W. Hongzhi, Z. Meifang, *Macromol. Mater. Eng.* **2017**, *302*, 1700214.

[22] H. L. Simons, U.S. 3280229, **1966**.

[23] D. Farrar, K. Ren, D. Cheng, S. Kim, W. Moon, W. L. Wilson, J. E. West, S. M. Yu, *Adv. Mater*. 2**011**, *23*, 3954.

[24] D. J. Lin, C. L. Chang, F. M. Huang, L. P. Cheng, *Polymer* **2003**, *44*, 413.

[25] A. Salimi, A. A. Yousefi, *J. Polym. Sci. B: Polym. Phys*. **2004**, *42*, 3487.

[26] X. Ma, J. Liu, C. Ni, D. C. Martin, D. B. Chase, J. F. Rabolt, *ACS Macro Lett*. **2012**, *1*, 428.

[27] R. Hasegawa, Y. Takahashi, Y. Chatani, H. Tadokoro, *Polym. J*. **1972**, *3*, 591.

[28] C. M. Roland, C. A. Bero, *Macromolecules* **1996**, *29*, 7521.

[29] J. Fialka, P. Benes, *IEEE Trans. Instrum. Meas.* **2013**, *62*, 1047.

[30] R. Song, G. Xia, X. Xing, L. He, Q. Zhao, Z. Mad, *J. Colloid Interface Sci.* **2013**, *401*, 50.

[31] C. M. Wu, M. H. Chou, *Compos. Sci. Technol.* **2016**, *127*, 127.

[32] Y. Huan, Y. Liu, Y. Yang, Y. Wu, *J. Appl. Polym. Sci.* **2007**, *104*, 858.

[33] J. T. L. Glenn, H. Zhaorong, *Smart Mater. Struct.* **2010**, *19*, 1.

[34] X. Liu, X. Kuang, S. Xu, X. Wang, *Mater. Lett.* **2017**, *191*, 189.

[35] Y. K. Fuh, J. C. Ye, P. C. Chen, H. C. Ho, Z. M. Huang, *ACS Appl. Mater. Interfaces* **2015**, *7*, 16923.

[36] X. Liu, M. Deng, X. Wang, *Mater. Lett.* **2017**, *189*, 66.

[37] X. Liu, S. Xu, X. Kuang, D. Tan, X. Wang, *RSC Adv*. **2016**, *6*, 109061.

[38] N. Soin, D. Boyer, K. Prashanthi, S. Sharma, A. A. Narasimulu, J. Luo, T. H. Shah, E. Sioresa, T. Thundat, *Chem. Commun*. **2015**, *51*, 8257.

[39] M. Sharma, V. Srinivas, G. Madras, S. Bose, *RSC Adv*. **2016**, *6*, 6251.

[40] K. Yao, F. E. H. Tay, *IEEE Trans. Ultrason. Eng.l* **2003**, *50*, 2.

[41] X. Li, Y. F. Lim, K. Yao, F. E. H. Tay, K. H. Seah, *Chem. Mater.* **2013**, *25*, 524.

[42] K. Tashiro, M. Kobayashi, H. Tadokoro, E. Fukada, *Macromolecules* **1980**, *13*, 691.

Published in: Advanced Electronic Materials, Vol. 4, No. 6, 1700562, DOI: 10.1002/aelm.201700562, Jun 2018

[43] W. Eisenmenger, H. Schmidt, B. Dehlen, *Braz. J. Phys.* **1999**, *29*, 295.

[44] G. Eberle, H. Schmidt, W. Eisenmenger, *IEEE Trans. Dielectr. Electr. Insul.* **1996**, *3*, 624.

[45] L. Yang, J. Ho, E. Allahyarov, R. R. Mu, L. Zhu, *ACS Appl. Mater. Interfaces* **2015**, *7*, 19894.

[46] S. Bauer, *IEEE Trans. Dielectr. Electr. Insul.* **2006**, *13*, 95.

Published in: Advanced Electronic Materials, Vol. 4, No. 6, 1700562, DOI: 10.1002/aelm.201700562, Jun 2018

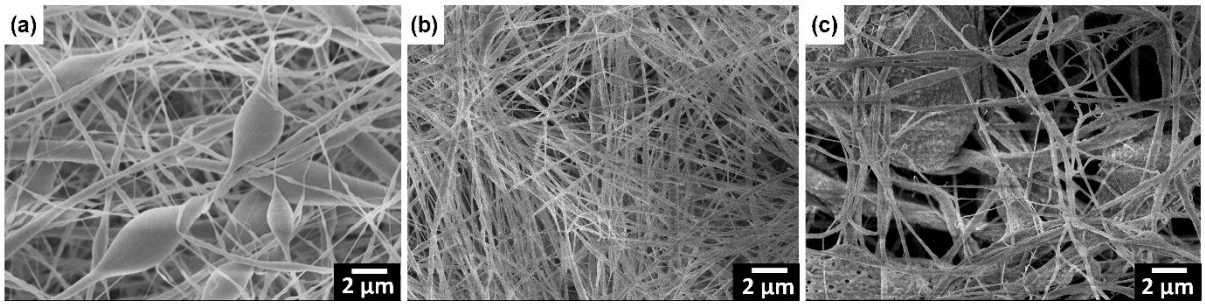

Figure 1: FESEM micrographs of the dried electrospun PVDF fibers **(a)** without Al $(NO_3)_3 \cdot 9H_2O$, **(b)** with 8 wt% Al $(NO_3)_3 \cdot 9H_2O$, and **(c)** with 16 wt% Al $(NO_3)_3 \cdot 9H_2O$.

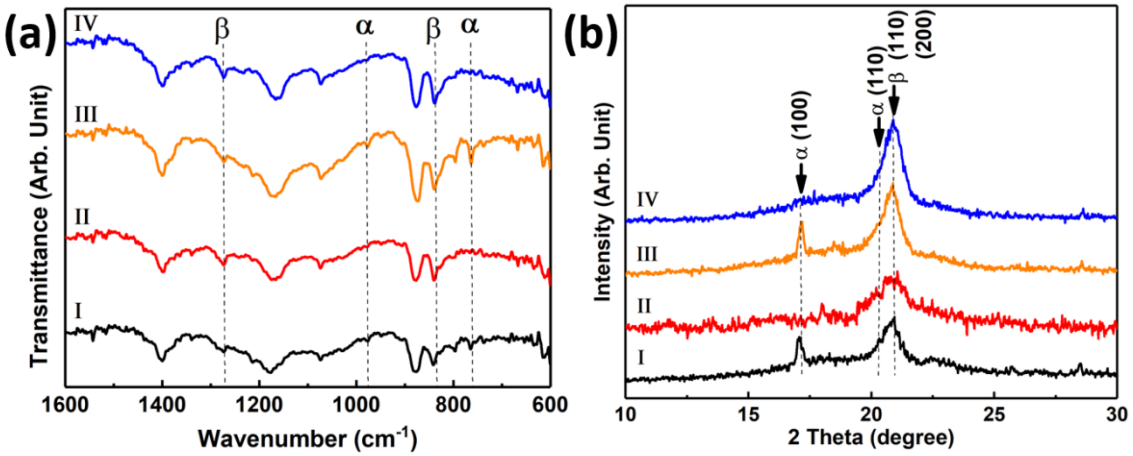

Figure 2: (a) FTIR spectra, **(b)** XRD patterns of PVDF films deposited by electrospinning and spin-coating process. (I) spin-coated film without Al $(NO_3)_3 \cdot 9H_2O$, (II) spin-coated film with 8 wt% Al $(NO_3)_3 \cdot 9H_2O$, (III) electrospun fibers without Al $(NO_3)_3 \cdot 9H_2O$, and (IV) electrospun fibers with 8 wt% Al $(NO_3)_3 \cdot 9H_2O$. The films were dried at 100 °C for 10 min followed by annealing at 135 °C for 12 hours. The unmarked peaks in the FTIR spectra are common to both α and β phases.

Published in: Advanced Electronic Materials, Vol. 4, No. 6, 1700562, DOI: 10.1002/aelm.201700562, Jun 2018

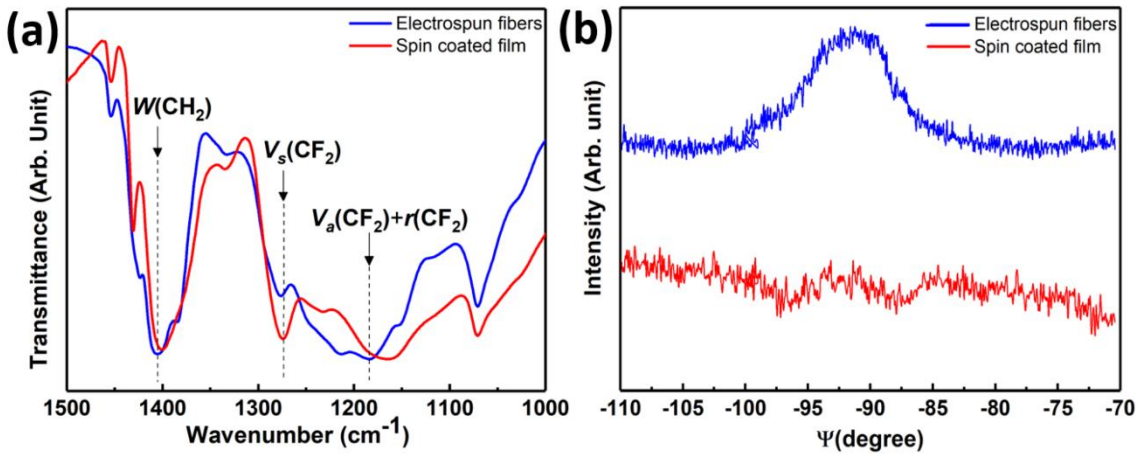

Figure 3: (a) Polarized FTIR spectra (normalized to absorption bands at 1400 cm^{-1}) for electrospun PVDF fibers in comparison with spin-coated film, and **(b)** ψ dependence of the XRD peak of β (110)/(200) reflections for electrospun PVDF fibers in comparison with spin-coated film. The fibers and the film were deposited from same solution of 15 wt% PVDF.

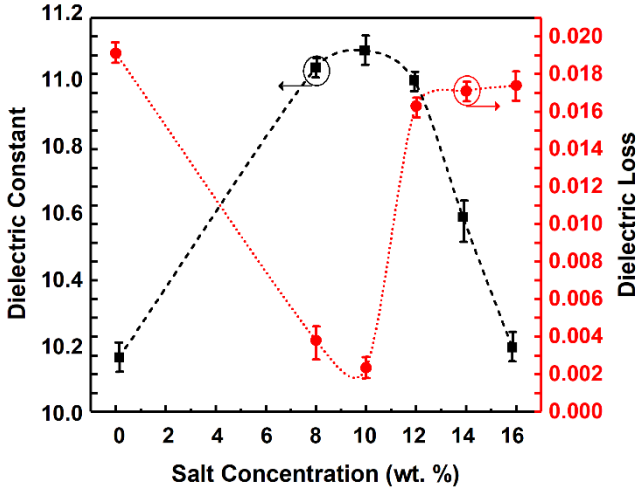

Figure 4: Dielectric constant and dielectric loss of electrospun PVDF fibers as a function of Al $(NO_3)_3 \cdot 9H_2O$ concentration, measured at 25 °C and 1 kHz.

Published in: Advanced Electronic Materials, Vol. 4, No. 6, 1700562, DOI: 10.1002/aelm.201700562, Jun 2018

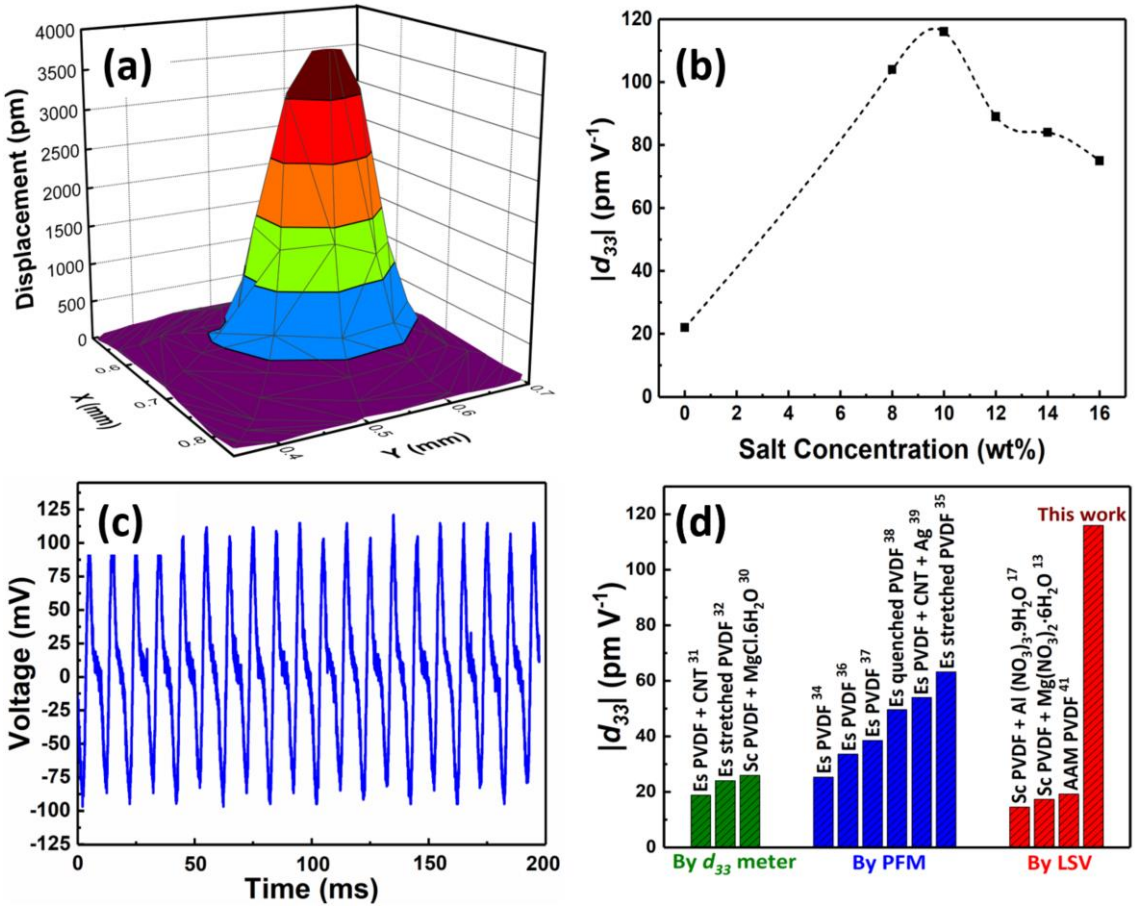

Figure 5: (a) Three-dimensional graph of instantaneous vibration obtained when the dilatation of the electrospun PVDF fibers reaches the maximum during the electric sine wave driving (30 V amplitude at 10 kHz). The sample is PVDF fiber film on Al substrate from solution with 10 wt% Al $(NO_3)_3 \cdot 9H_2O$. The central protruded area is the electrically excited fibers under the top Al electrode, whereas the flat adjacent area is the PVDF fibers without the top electrode. **(b)** The effective $d_{33\,(eff)}$ values of electrospun PVDF fibers with different Al $(NO_3)_3 \cdot 9H_2O$ concentrations. **(c)** Voltage output of electrospun PVDF fibers from solution with 10 wt% Al $(NO_3)_3 \cdot 9H_2O$ at a cyclic vibration frequency of 100 Hz. **(d)** Comparison of the reported d_{33} values in literature for various PVDF homopolymer films: Es stands for electrospinning, Sc stands for spin coating, and AAM stands for anodic alumina membrane.

Published in: Advanced Electronic Materials, Vol. 4, No. 6, 1700562, DOI: 10.1002/aelm.201700562, Jun 2018

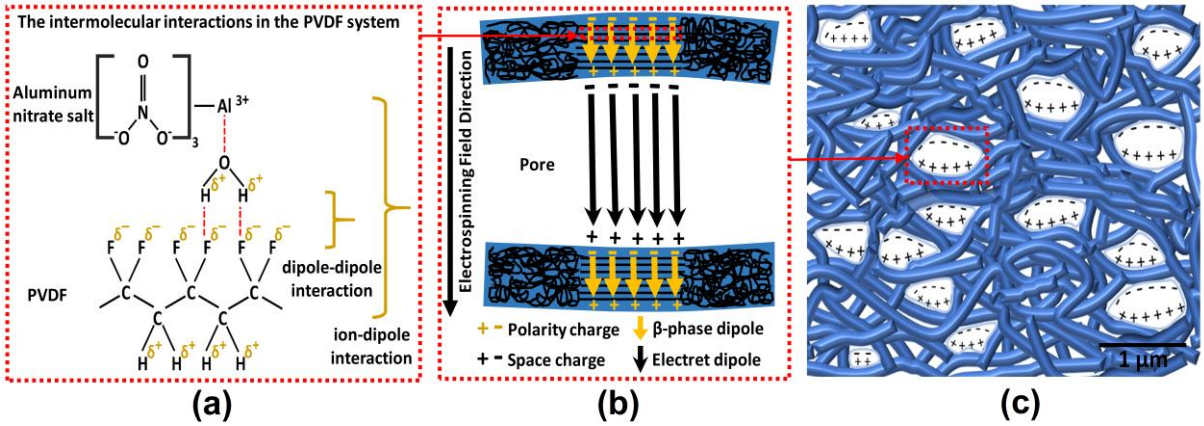

Figure 6: (a) The intermolecular interactions of PVDF with ($Al(NO_3)_3 \cdot 9H_2O$) salt, **(b)** schematic illustration of two bundles of electrospun PVDF nanofibers containing oriented polar crystals and amorphous phases and formation of space charges at the polarized surfaces between fibers, and **(c)** formation of charged voids between the nanofibers.

Published in: Advanced Electronic Materials, Vol. 4, No. 6, 1700562, DOI: 10.1002/aelm.201700562, Jun 2018

Giant effective piezoelectric strain and voltage coefficients are achieved in electrospun PVDF nanofibers from solution modified by hydrated salt. The investigation clarifies a synergistic interactive mechanism involving the hydrated salt and the electric field during electrospinning leading to polarization enhancement and alignment, showing a strategy in achieving high performance functional polymeric materials through dedicated control in their nanostructures and polarizations.

Keyword: piezoelectric, polarization, PVDF, electromechanical, nanofibers

Y. M. Yousry, K. Yao*, S. Chen, W. H. Liew, S. Ramakrishna.

Title: Mechanisms for Enhancing Polarization Orientation and Piezoelectric Parameters of PVDF Nanofibers